Desalination and Water Treatment
www.deswater.com

doi: 10.1080/19443994.2014.954147

56 (2015) 1940–1948
November

Taylor & Francis
Taylor & Francis Group

Environmental remediation of aqueous cyanide by photocatalytic oxidation using a $NiFe_2O_4/TiO_2$–SiO_2 core–shell nanocomposite

Mohammad W. Kadi[a], R.M. Mohamed[a,b,c,*]

[a]*Faculty of Science, Department of Chemistry, King Abdulaziz University, P.O. Box 80203, Jeddah 21589, Saudi Arabia, Tel. +96 626952293; Fax: +96 626952292; email: redama123@yahoo.com (R.M. Mohamed)*
[b]*Advanced Materials Department, Central Metallurgical R&D Institute, CMRDI, P.O. Box 87 Helwan, Cairo 11421, Egypt*
[c]*Center of Excellence in Environmental Studies, King Abdulaziz University, P.O. Box 80216, Jeddah 21589, Saudi Arabia*

Received 18 February 2014; Accepted 6 August 2014

ABSTRACT

A core–shell $NiFe_2O_4/SiO_2$–TiO_2 nanocomposite photocatalyst was prepared in a three-stage manner. The $NiFe_2O_4$ core was prepared by applying an organic precursor method. This core was coated with SiO_2 and then with TiO_2. The optimum preparation conditions were determined by examining various molar ratios of Si, Ti, ethanol, and ammonia. X-ray powder diffraction, DR-UV, TEM, and magnetization techniques were used to characterize the nanocomposite. Using molar ratios of $SiO_2/NiFe_2O_4$ = 0.03, ethanol/$NiFe_2O_4$ = 20, ammonia/$NiFe_2O_4$ = 1, and Ti/ethanol = 0.8, a magnetic photocatalyst of enhanced properties was synthesized. A surface area of 520 m^2/g, saturation magnetization value of 53.2 amu/g, coercivity of 500.0 Oe, and a band gap of 2.54 eV were observed for the synthesized $NiFe_2O_4/SiO_2$–TiO_2 nanocomposite photocatalyst. These characteristics allowed excellent photodegradation of the toxic cyanide ion. In addition, the strong magnetic properties allow for the efficient reuse of the catalyst.

Keywords: Core–shell; Visible photocatalyst; Cyanide

1. Introduction

Titania and titania-based nanoparticles are promising photocatalysts in environmental remediation and pollutant treatment. Many researchers have successfully used titania and its combinations for the removal of industrial and domestic pollutants [1–3]. Nakata and Fujishima published an extensive review of TiO_2 as a nanocatalyst, its applications, and recent publications [4]. The properties that define the photocatalytic efficiency of a material include its particle size, band gap energy, pore size, stability, hole–pair recombination rate, and other properties [5]. To enhance favorable properties, researchers combine other oxides with TiO_2, dope TiO_2 with p- and n-type semiconductors, control physical and chemical conditions during TiO_2 preparation, and explore new preparation methods [6–12].

Combining TiO_2 and SiO_2 to produce a photocatalyst has attracted the attention of many researchers due to the stability of both oxides, low cost, absence of environmental risks, and the ample room for manipulation and enhancement of desired properties. Ren et al. reported a highly active TiO_2/SiO_2 catalyst with a 63% benzene conversion rate [13]. A sol–gel-prepared TiO_2/SiO_2 photocatalyst was used for cyanide

*Corresponding author.

degradation in aqueous media [14]. Jaroenworaluck et al. showed that the degree of UV absorption of a TiO_2/SiO_2 photocatalyst is related to particle size, surface characteristics, and the percent of TiO_2 loading [15]. Cai et al. prepared a high-surface-area TiO_2/SiO_2 photocatalyst by employing a dual-templating technique [16]. Cetinkaya et al. prepared an effective TiO_2/SiO_2 photocatalyst for the degradation of acid orange [17]. An important shortcoming in the effective application of an otherwise excellent photocatalyst is the difficulty of removing the nanoparticles from the solution after the photocatalysis process. The immobilization of the catalyst by its fixation onto inert substrates, such as glass beads, silica gel, sand, and other materials, can be used to overcome this disadvantage [18–21].

In recent years, core–shell morphology has emerged as an attractive method for the design of photocatalysts for environmental applications. In core–shell morphology, a magnetic core material provides a means of magnetic separation of the catalyst, while manipulation of the shell material allows for the enhancement of the desired photocatalytic properties [22–24]. Nickel ferrite ($NiFe_2O_4$) is a magnetic material suitable for use in the core–shell preparations of new materials. It has been used as a catalyst and in many other applications [25,26]. The objective of this work is the removal of toxic cyanide ions from wastewater using a magnetic photocatalyst that can be easily separated and reused many times. Therefore, in this work we report the synthesis of a magnetically separable TiO_2–$SiO_2/NiFe_2O_4$ core–shell structure. We also report the optimization of the synthesis conditions to produce particles with enhanced photocatalytic activity and the application of these particles to CN^- degradation in an aqueous medium.

2. Experimental

2.1. Synthesis of the nickel ferrite core

Nickel ferrite particles were prepared via the organic acid precursor method using Fe $(NO_3)_3{\cdot}9H_2O$ (purity 99%) and Ni $(NO_3)_2{\cdot}6H_2O$ (purity 98.3%) as iron and nickel sources. Synthesis parameters were optimized to produce particles with the best magnetic and surface area properties. The details of the experimental procedure and optimization conditions can be found elsewhere [27].

2.2. Incorporation of the titania–silica shell

In this part of the procedure, the $NiFe_2O_4$ core was first coated with silica followed by coating the resultant $NiFe_2O_4/SiO_2$ with TiO_2. In the first step, tetraethyl orthosilicate (TEOS, ≥98%) was used. Coating the $NiFe_2O_4$ with SiO_2 can be summarized in the following steps: disperse the $NiFe_2O_4$ particles in absolute ethanol; add H_2O required for the hydrolysis process and stir for 20 min; add NH_4OH to the mixture under vigorous stirring and stir for another 20 min; add an appropriate amount of TEOS dropwise; let the solution stand for 24 h for complete aging of the SiO_2; wash the product and centrifuge first using H_2O (three times) and then ethanol (two times); and dry the product for 1 d at 60˚C. The second step involves coating with TiO_2. Titanium tetrabutoxide (TBOT, ≥98%) was used as a source of TiO_2. This second coating procedure can be summarized in the following steps: Disperse the $NiFe_2O_4/SiO_2$ in ethanol (0.125 g/25 mL) using an ultrasonic bath for 30 min at 20˚C. Transfer the dispersion to a mixture of 35 mL of ethanol +25 mL of water. Dissolve an appropriate amount of TBOT in 40 mL of ethanol and then transfer it dropwise to the dispersion. The final concentration of TBOT should equal 0.04. Continue the vigorous stirring for 3 h at room temperature. Let the solution stand overnight and then wash and centrifuge using H_2O and ethanol. Dry the product for 2 d at 60˚C.

2.3. Characterization and optimization of synthesis parameters

The $NiFe_2O_4/SiO_2$–TiO_2 core–shell samples thus produced were evaluated and characterized by employing various techniques to determine their properties. Magnetic properties were determined using a vibrating sample magnetometer (VSM; 9600–1 LDJ, USA) at room temperature in a maximum applied field of 15 kOe. Saturation magnetization (M_s) and coercivity (H_c) were determined from the hysteresis loops thus obtained. X-ray powder diffraction (XRD) patterns of the calcined products were obtained with a Bruker axis D8 using a Cu Ka radiation (k = 1.540 Å). The average crystallite sizes of the powders were estimated automatically from the corresponding XRD data using the Scherrer formula. A twin-beam Perkin-Elmer Lambda 800 UV/Vis spectrometer was used to determine the particle band gap profile. In a twin-beam instrument, the beam that passes through a target sample is compared to a control sample. The absorption is determined by the intensity difference of the two beams. Bandgap profiles were approximated by fitting the data using the Tauc relation. N_2-adsorption measurement was carried out at 77 K using a Nova 2000 series Chromatech for surface area analysis.

The optimization of the synthesis parameters was investigated by examining various experimental conditions. The effects of the silica/nickel ferrite molar ratio, ethanol/nickel ferrite molar ratio, ammonia/nickel ferrite molar ratio, and titanium/ethanol molar ratio were systematically studied. After synthesis under each condition, a full characterization was performed, and the resulting properties were examined. The optimal synthesis parameters that produced the most desired properties were deduced.

2.4. Photocatalytic reaction studies

The catalyst prepared under optimal conditions was tested using the photodegradation of cyanide under visible light as a measure of its photocatalytic activity. Photodegradation experiments were carried out in a horizontal cylindrical annular batch reactor. The photocatalyst–cyanide mixture was irradiated with a 150 W blue fluorescent lamp with a UV cutoff filter in place. In a typical experiment, a certain weight of the catalyst is suspended in a 300 mL of a 100 mg/L KCN solution (at pH 10.5, to avoid the evolution of HCN gas). The reaction was carried out isothermally at 25°C, and the reaction mixture was sampled at different intervals for a total reaction period of 1 h. The $CN^-_{(aq)}$ concentration was estimated by volumetric titration with $AgNO_3$, using KI to determine the titration end-point. The removal efficiency of CN^- was measured by applying the following equation:

$$\% \text{ Removal efficiency} = \frac{(C_0 - C)}{C_0} \times 100 \quad (1)$$

where C_0 is the initial concentration of uncomplexed CN^- and C is the concentration of unoxidized CN^- in the solution.

3. Results and discussion

Preliminary studies showed that controlling the quantities of reactants in the synthesis procedure affects the properties of the final product. Thus, a detailed examination of the synthesis procedure was performed altering the ratios of certain reactants. The effects of silica/nickel ferrite, ethanol/nickel ferrite, ammonia/nickel ferrite, and titanium/ethanol molar ratios on surface area, magnetic properties, band gap energy, morphology, and the crystalline phase of TiO_2 in the nanocatalyst produced under the experimental conditions were systematically studied.

3.1. Effect of silica/nickel ferrite molar ratio

In this optimization step, a series of experiments was carried out by changing the silica/nickel ferrite molar ratios from 0.01 to 0.04 under the following conditions:

In the first step, we used a molar ratio of 20 for ethanol/nickel ferrite, a molar ratio of 1.0 for ammonia/nickel ferrite, and a 60°C drying temperature for 1 d. In the second step, we used a molar ratio of 0.04 for TBOT/ethanol, a 60°C drying temperature for 1 d, and a 550°C crystallization temperature for 3 h.

The examination of the XRD patterns of pure $NiFe_2O_4$ and $NiFe_2O_4/SiO_2$–TiO_2 composites synthesized by changing the $SiO_2/NiFe_2O_4$ molar ratios reveal a biphasic nature of the prepared samples. The diffraction patterns observed in Fig. 1 show peaks corresponding to planes (1 1 1), (2 2 0), (3 1 1), (2 2 2), (4 0 0), (4 2 2), and (3 3 3), confirming the formation of spinel nickel ferrite (JCPDS Patterns No. 44–1485). Diffraction peaks corresponding to planes (1 0 1), (0 0 4), and (2 0 0) of anatase titanium oxide appear in the TiO_2-coated samples.

The magnetic parameter values (Table 1) show that coated samples can be regarded as moderately hard ferromagnetic materials due to their high coercive force of 215–493 Oe and high remanence values of 3.8–15.9 emu/g. These values, along with the high saturation magnetization (M_s = 42.7 emu/g) obtained at a silica/$NiFe_2O_4$ molar ratio of 0.03, imply that the photocatalyst can be easily collected magnetically and re-dispersed in a solution for reuse.

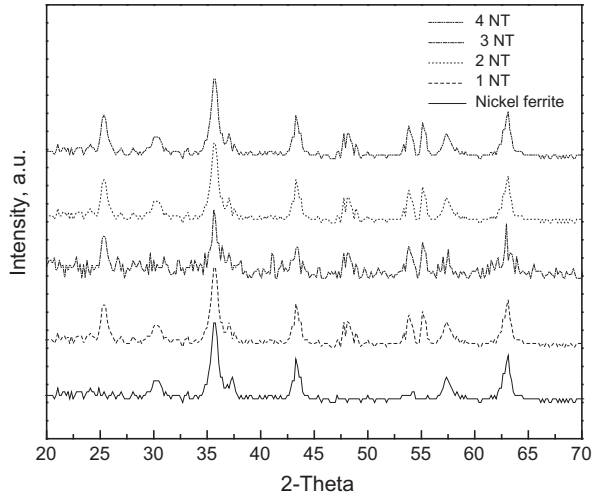

Fig. 1. X-ray patterns of pure $NiFe_2O_4$ and $NiFe_2O_4/SiO_2$–TiO_2 composites synthesized at different $SiO_2/NiFe_2O_4$ molar ratios.

Table 1
Observed and calculated characteristics of pure $NiFe_2O_4$ and $NiFe_2O_4/SiO_2$–TiO_2 composites synthesized at different $SiO_2/NiFe_2O_4$ molar ratios

Sample	$SiO_2/NiFe_2O_4$ molar ratio	Phases formed	M_r (emu/g)	M_s (emu/g)	H_c (Oe)	Band gap (eV)	CN^- removal efficiency (%)	BET (m^2/g)
$NiFe_2O_4$*	–	$NiFe_2O_4$	39.2	61.8	942.0	–	–	–
1 NT	0.01	$NiFe_2O_4$ + TiO_2 anatase	3.8	15.3	215.6	2.97	65	320
2 NT	0.02	$NiFe_2O_4$ + TiO_2 anatase	6.9	23.5	311.7	2.80	89	400
3 NT	0.03	$NiFe_2O_4$ + TiO_2 anatase	15.9	42.7	493.0	2.66	100	480
4 NT	0.04	$NiFe_2O_4$ + TiO_2 anatase	13.2	37.5	341.1	2.64	100	490

*Synthesized under optimum conditions [27].

TEM images of $NiFe_2O_4/SiO_2$–TiO_2 composites synthesized at different $SiO_2/NiFe_2O_4$ molar ratios are shown in Fig. 2. The figure shows that by increasing the TEOS molar ratio from 0.01 to 0.03, the amount of precipitated silica increases, and the particle size of the core–shell becomes smaller (Fig. 3(c)) due to the amorphous nature of the silica and its high surface area. However, with a molar ratio greater than 0.03 (i.e. sample 4 NT, Fig. 3(d)), it seems that the titania–silica shell separates from the core.

The DR-UV spectra of the $NiFe_2O_4/SiO_2$–TiO_2 composites synthesized at different $SiO_2/NiFe_2O_4$

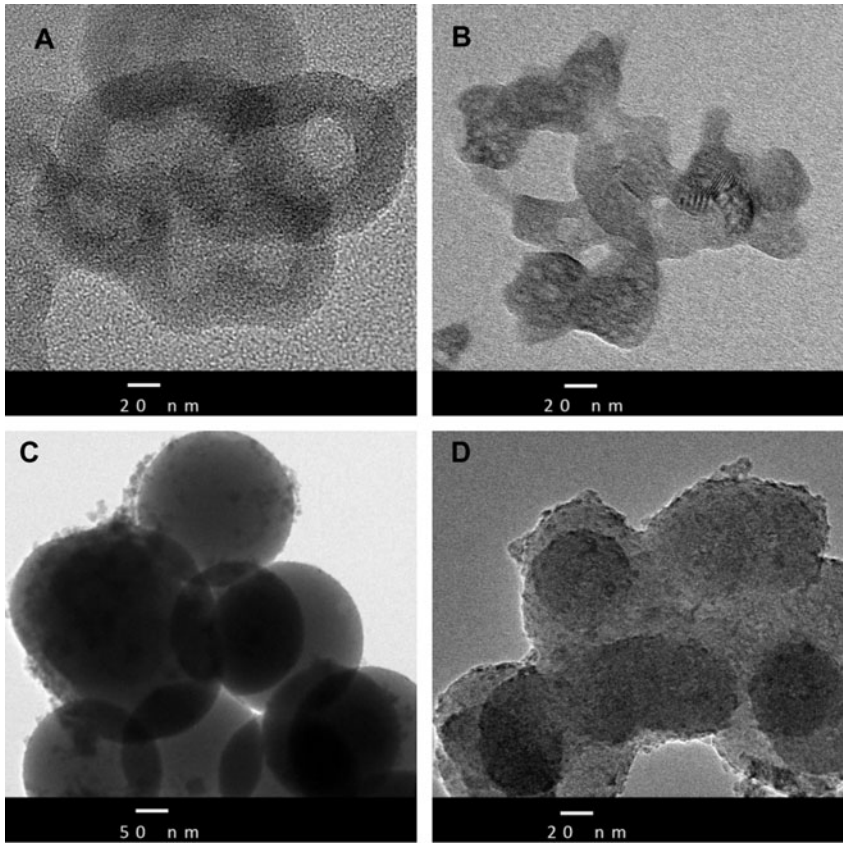

Fig. 2. TEM images of $NiFe_2O_4/SiO_2$–TiO_2 composites synthesized at different $SiO_2/NiFe_2O_4$ molar ratios.

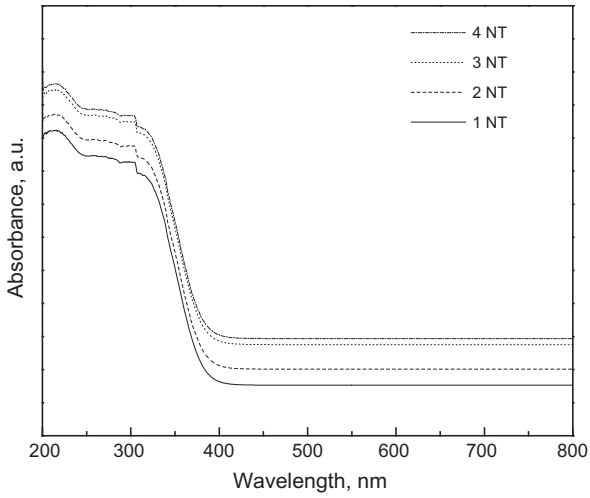

Fig. 3. UV–vis spectra of $NiFe_2O_4/SiO_2$–TiO_2 composites synthesized at different $SiO_2/NiFe_2O_4$ molar ratios.

molar ratios are shown in Fig. 3. An estimate of the optical band gap is obtained using the equation:

$$\alpha(h\gamma) = A(h\gamma - E_g)^{m/2} \quad (2)$$

where A is a constant, α is the absorption coefficient, and m equals 1 for a direct transition. The energy intercept of a plot of $(\alpha\ h\gamma)^2$ vs. $(h\gamma)$ yields E_g for a direct transition. The band gap values calculated for the various samples are presented in Table 1. The results show that an increase in the $TiO_2/NiFe_2O_4$ molar ratio from 0.01 to 0.03 decreases the band gap of the samples produced from 2.97 to 2.66 eV; however, no significant effect on the band gap is observed by a further increase in the molar ratio.

It is clear from Table 1 that a $SiO_2/NiFe_2O_4$ molar ratio of 0.03 produces the best composite with a high surface area, strong magnetic properties, low band gap, and an excellent CN^- degradation ability under illumination with visible light. Therefore, in subsequent preparations, we adopted the preparation conditions for sample 3NT (Fig. 3(c)) as the optimum for this factor due to its high surface area, low band gap, and high magnetization properties.

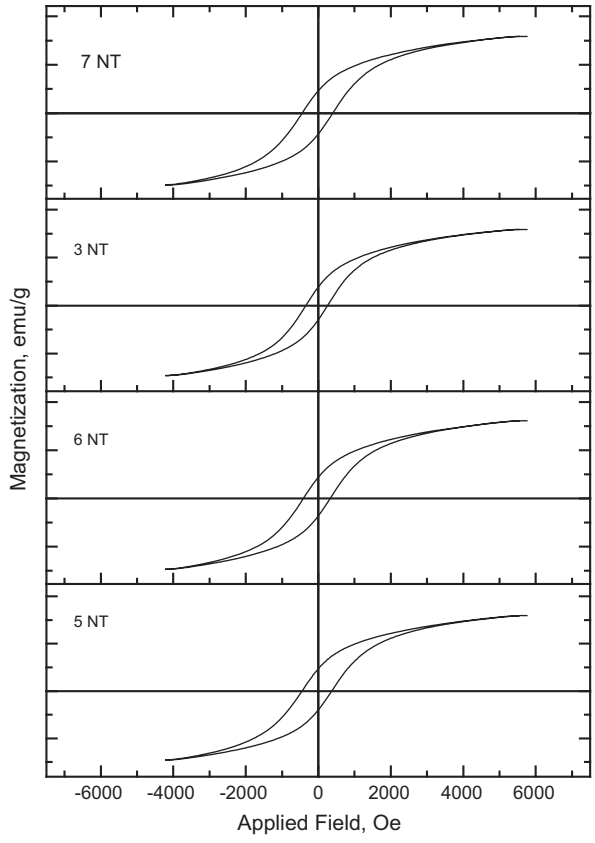

Fig. 4. Effect of the ethanol/nickel ferrite molar ratio on the M–H hysteresis loops of synthesized $NiFe_2O_4/SiO_2$–TiO_2.

Table 2
Observed and calculated characteristics of $NiFe_2O_4/SiO_2$–TiO_2 composites synthesized at different ethanol/$NiFe_2O_4$ molar ratios

Sample	Ethanol/$NiFe_2O_4$ molar ratio	Phases formed	M_r (emu/g)	M_s (emu/g)	H_c (Oe)	Band gap (eV)	CN^- removal efficiency (%)	BET (m^2/g)
5 NT	5	$NiFe_2O_4$ + TiO_2 anatase	33.0	10.1	340.5	3.02	88	330
6 NT	10	$NiFe_2O_4$ + TiO_2 anatase	29.1	8.9	348.8	2.91	97	390
3 NT	20	$NiFe_2O_4$ + TiO_2 anatase	42.7	15.9	493.0	2.66	100	480
7 NT	30	$NiFe_2O_4$ + TiO_2 anatase	11.1	3.8	427.7	2.82	90	350

3.2. Effect of ethanol/nickel ferrite molar ratio

For this molar ratio examination, the $NiFe_2O_4$/SiO_2–TiO_2 composites were synthesized at molar ratios of 5, 10, 20, and 30 for ethanol/nickel ferrite, while keeping all other conditions unchanged and setting the SiO_2/$NiFe_2O_4$ molar ratio at 0.03, as deduced from Section 3.1.

The hysteresis loops obtained from magnetization measurements of the ferrite powders of $NiFe_2O_4$/SiO_2–TiO_2 composites synthesized at molar ratios of 5, 10, 20, and 30 for ethanol/nickel ferrite are shown in Fig. 4. A summary of the characteristics of these composites compared with sample 3 NT from the previous section is presented in Table 2. It is clear from Table 2 that an ethanol/$NiFe_2O_4$ molar ratio of 20 produces a

Table 3
Observed and calculated characteristics of $NiFe_2O_4$/SiO_2–TiO_2 composites synthesized at different ammonia/$NiFe_2O_4$ molar ratios

Sample	Ammonia/$NiFe_2O_4$ molar ratio	Phases formed	M_r (emu/g)	M_s (emu/g)	H_c (Oe)	Band gap (eV)	CN^- removal efficiency (%)	BET (m^2/g)
8 NT	0.4	$NiFe_2O_4$ + TiO_2 anatase	19	6.5	411.0	3.07	89	400
9 NT	0.8	$NiFe_2O_4$ + TiO_2 anatase	5.7	2.1	498.0	2.88	93	410
3 NT	1	$NiFe_2O_4$ + TiO_2 anatase	42.7	15.9	493.0	2.66	100	480
10 NT	1.2	$NiFe_2O_4$ + TiO_2 anatase	38.6	10.5	403.0	2.74	89	360

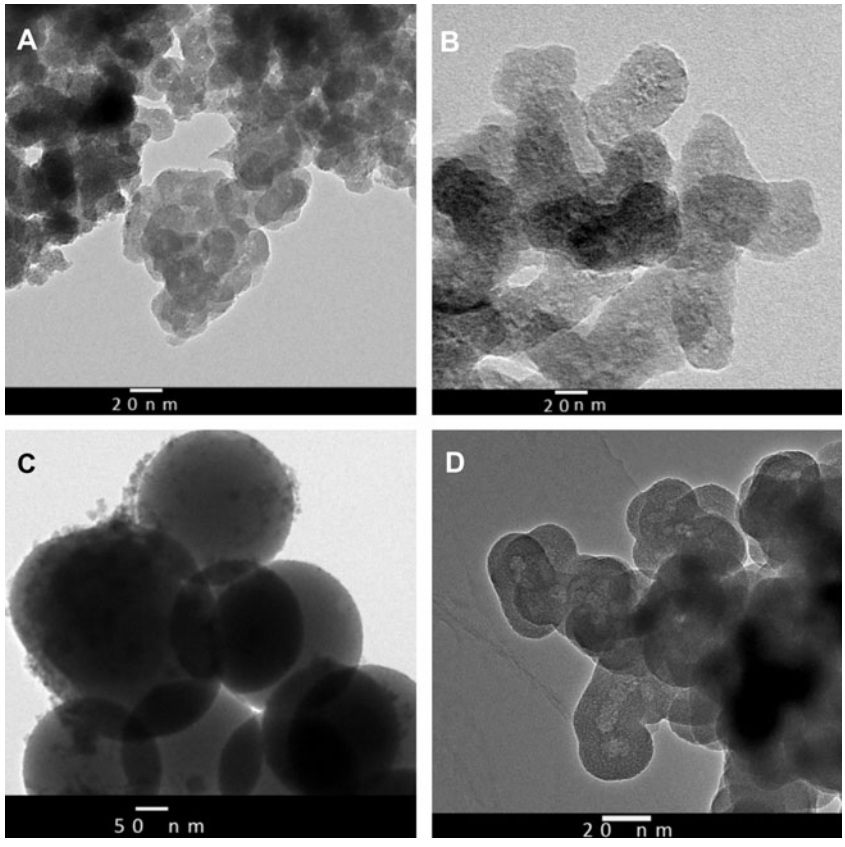

Fig. 5. TEM images of calcined $NiFe_2O_4$/SiO_2–TiO_2 composites synthesized at different ammonia/$NiFe_2O_4$ molar ratios.

Table 4
Observed and calculated characteristics of $NiFe_2O_4/SiO_2$–TiO_2 composites synthesized at different Ti/ethanol molar ratios

Sample	Ti/ethanol molar ratio	Phases formed	M_r (emu/g)	M_s (emu/g)	H_c (Oe)	Band gap (eV)	CN^- removal efficiency (%)	BET (m^2/g)
3 NT	0.04	$NiFe_2O_4$ + TiO_2 anatase	42.7	15.9	493.0	2.66	100	480
11 NT	0.08	$NiFe_2O_4$ + TiO_2 anatase	53.2	20.3	500.0	2.54	100	520
12 NT	0.16	$NiFe_2O_4$ + TiO_2 anatase	17.4	6.2	430.0	2.76	88	390
13 NT	0.32	$NiFe_2O_4$ + TiO_2 anatase	14.1	4.7	410.0	2.95	82	360

$NiFe_2O_4/SiO_2$–TiO_2 composite with the best characteristics. Decreasing this ratio results in compromising some of the desired properties. For example, the band gap increases to 2.91 and 3.02 eV with ratios of 10 and 5, respectively. Magnetic properties were also compromised. An increase of the molar ratio beyond 20 also produced undesirable results. Thus, in all subsequent preparations, the ethanol/$NiFe_2O_4$ molar ratio of 20 was adopted due to the high surface area, low band gap, and high magnetization properties of the product.

3.3. Effect of ammonia/nickel ferrite molar ratio

Setting the $SiO_2/NiFe_2O_4$ molar ratio at 0.03 and ethanol/$NiFe_2O_4$ molar ratio at 20, synthesis was performed using ammonia/$NiFe_2O_4$ molar ratios of 0.4, 0.8, 1, and 1.2. Table 3 summarizes the characteristics of the $NiFe_2O_4/SiO_2$–TiO_2 composites thus produced. The numbers in Table 3 show that by increasing the ammonia/$NiFe_2O_4$ molar ratio, all properties are enhanced up to a molar ratio of 1. Beyond that value properties are compromised. This indicates that a molar ratio of 1 for ammonia/$NiFe_2O_4$ is the most favorable experimental ratio. Furthermore, TEM images of $NiFe_2O_4/SiO_2$–TiO_2 composites synthesized at different ammonia/$NiFe_2O_4$ molar ratios (Fig. 5) show that increasing the molar ratio for the ammonia hydrolysis process improves the silica precipitation producing smaller silica particles as in Fig. 5(a), (b), and (c). However, in Fig. 5(d) (with a ratio of 1.2), the agglomeration of silica particles separate the shell from the magnetic core. Hence, the optimum condition is when the ratio is 1.0 (Fig. 5(c)). This condition shows the smallest core–shells, indicating a high surface area. The best efficiency plus good magnetic properties are also evident from Table 3.

3.4. Effect of titanium/ethanol molar ratio

Setting the $SiO_2/NiFe_2O_4$ molar ratio at 0.03, the ethanol/$NiFe_2O_4$ molar ratio at 20, and the ammonia/$NiFe_2O_4$ molar ratio at 1, the effect of changing the Ti/ethanol molar ratio was examined. Syntheses were performed using Ti/ethanol molar ratios of 0.04, 0.08, 0.16, and 0.32. The product characteristics deduced from XRD, magnetization, DR-UV spectra, CN^- degradation examination, and surface area measurements are presented in Table 4. A biphasic mixture of nickel ferrite and anatase phases forms in all trials. The intensity of the nickel ferrite decreases with the increase in the Ti/ethanol molar ratio (Fig. 6). The magnetic properties deduced from hysteresis loops indicate that the $NiFe_2O_4/SiO_2$–TiO_2 composites possess high coercive force values ranging from 410 to

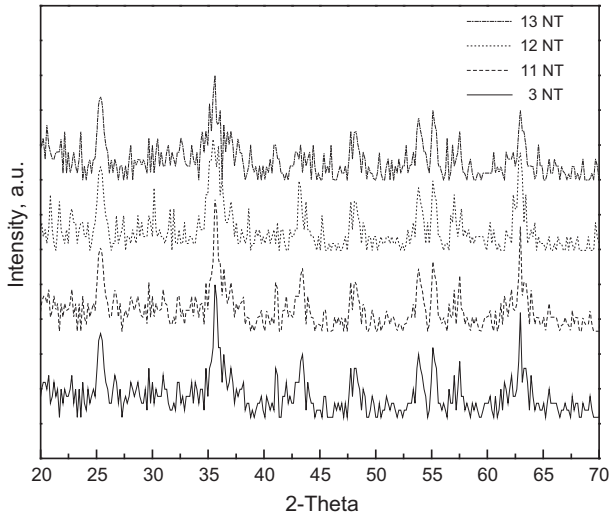

Fig. 6. X-ray patterns of $NiFe_2O_4/SiO_2$–TiO_2 composites synthesized at different Ti/ethanol molar ratios.

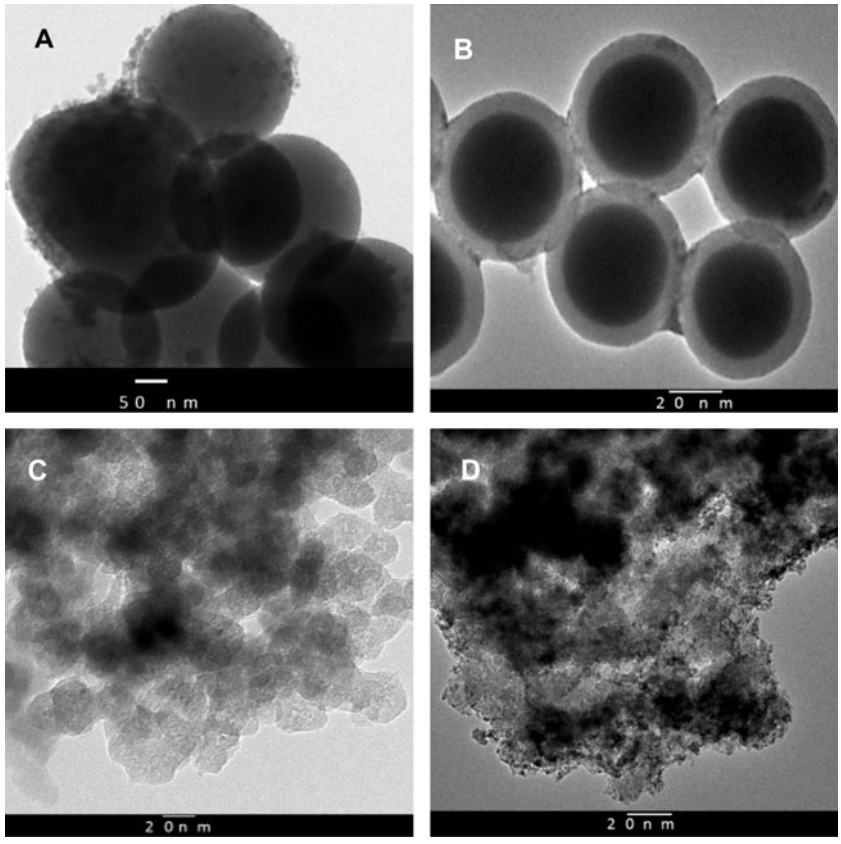

Fig. 7. TEM images of calcined $NiFe_2O_4/SiO_2$–TiO_2 composites synthesized at different Ti/ethanol molar ratios.

500 Oe and high remanence values of 4.7–20.3 emu/g, indicating that the separation from the suspension can easily be achieved magnetically. The highest saturation magnetization (53.2 emu/g) was obtained at a titanium/ethanol molar ratio of 0.08, indicating that this ratio is optimum for the synthesis of $NiFe_2O_4/SiO_2$–TiO_2 composites. Calculations from the DR-UV spectra of $NiFe_2O_4/SiO_2$–TiO_2 composites show that an increase in the Ti/ethanol molar ratio from 0.04 to 0.08 decreases the band gap of the composites thus produced from 2.66 to 2.54 eV. However, a further increase in the Ti/ethanol ratio results in an increase of the band gap. The TEM images of $NiFe_2O_4/SiO_2$–TiO_2 composites prepared at different Ti/ethanol molar ratios are shown in Fig. 7. The figure shows that by increasing the TBOT, the attractive forces between silica and titania increase, allowing shell separation from the magnetic core. This affects both the magnetic properties and the efficiency of the catalyst. All factors considered, one can conclude that a TBOT molar ratio of 0.08 (Fig. 7(b)) is the optimum at which favorable properties of the catalyst are enhanced.

4. Conclusions

$NiFe_2O_4$ was prepared via the organic acid precursor method. This magnetic core was coated with SiO_2 and TiO_2 in a two-stage manner. Synthesis conditions were optimized by varying the $SiO_2/NiFe_2O_4$, ethanol/$NiFe_2O_4$, ammonia/$NiFe_2O_4$, and Ti/ethanol molar ratios. Optimum molar ratios were found to be 0.03, 20, 1, and 0.8, respectively. Applying these optimal ratios and other experimental parameters, a core–shell $NiFe_2O_4/SiO_2$–TiO_2 photocatalyst was synthesized. The photocatalytic efficiency of the catalyst was tested on the CN^- photodegradation reaction under visible light illumination. A high percent removal of CN^- was achieved.

References

[1] F. Deng, Y. Li, X. Luo, L. Yang, X. Tu, Preparation of conductive polypyrrole/TiO_2 nanocomposite via surface molecular imprinting technique and its photocatalytic activity under simulated solar light irradiation, Colloids Surf., A 395 (2012) 183–189.

[2] Y. Cao, Y. Yu, P. Zhang, L. Zhang, T. He, Y. Cao, An enhanced visible-light photocatalytic activity of TiO_2 by nitrogen and nickel–chlorine modification, Sep. Purif. Technol. 104 (2013) 256–262.
[3] M. Farrokhi, J. Yang, S. Lee, M. Shirzad-Siboni, Effect of organic matter on cyanide removal by illuminated titanium dioxide or zinc oxide nanoparticles, J. Environ. Health Sci. Eng. 11 (2013) 23–28.
[4] K. Nakata, A. Fujishima, TiO_2 photocatalysis: Design and applications, J. Photochem. Photobiol., C 13 (2012) 169–189.
[5] R.M. Mohamed, D.L. McKinney, W.M. Sigmund, Enhanced nanocatalysts, Mater. Sci. Eng., R 73 (2012) 1–13.
[6] R.M. Mohamed, E.S. Baeissa, Mordenite encapsulated with Pt-TiO_2: Characterization and applications for photocatalytic degradation of direct blue dye, J. Alloys Compd. 558 (2013) 68–72.
[7] R.M. Mohamed, E. Aazam, Synthesis and characterization of P-doped TiO_2 thin-films for photocatalytic degradation of butyl benzyl phthalate under visible-light irradiation, Chin. J. Catal. 34 (2013) 1267–1273.
[8] R.M. Mohamed, UV-assisted photocatalytic synthesis of TiO_2-reduced graphene oxide with enhanced photocatalytic activity in decomposition of sarin in gas phase, Desalin. Water Treat. 50 (2012) 147–156.
[9] R.M. Mohamed, E.S. Aazam, Preparation and characterization of platinum doped porous titania nanoparticles for photocatalytic oxidation of carbon monoxide, J. Alloys Compd. 509 (2011) 10132–10138.
[10] R.M. Mohamed, I.A. Mkhalid, Characterization and catalytic properties of nano-sized Ag metal catalyst on TiO_2–SiO_2 synthesized by photo-assisted deposition and impregnation methods, J. Alloys Compd. 501 (2010) 301–306.
[11] R.M. Mohamed, I.A. Mkhalid, The effect of rare earth dopants on the structure, surface texture and photocatalytic properties of TiO_2–SiO_2 prepared by sol-gel method, J. Alloys Compd. 501 (2010) 143–147.
[12] R.M. Mohamed, S. Elham Aazam, Characterization and catalytic properties of nano-sized Au metal catalyst on titanium containing high mesoporous silica (Ti-HMS) synthesized by photo-assisted deposition and impregnation methods, Int. J. Photoenergy 2011 (2011) 1–7. Article ID 137328.
[13] C. Ren, W. Qiu, Y. Chen, Physicochemical properties and photocatalytic activity of the TiO_2/SiO_2 prepared by precipitation method, Sep. Purif. Technol. 107 (2013) 264–272.
[14] M. Siboni, M.R. Samarghandi, J.-K. Yang, S.-M. Lee, Photocatalytic removal of cyanide with illuminated TiO_2, Water Sci. Technol. 64 (2011) 1383–1387.
[15] A. Jaroenworaluck, N. Pijarn, N. Kosachan, R. Stevens, Nanocomposite TiO_2–SiO_2 gel for UV absorption, Chem. Eng. J. 181–182 (2012) 45–55.
[16] T. Cai, Y. Wang, Y. Dong, X. Li, Z. Liu, Z. Yan, Synthesis of hierarchically ordered egg-tray-like macroporous TiO_2–SiO_2 nanocomposites with ordered mesoporous walls, Mater. Lett. 111 (2013) 173–176.
[17] T. Cetinkaya, L. Neuwirthová, K.M. Kutláková, V. Tomášek, H. Akbulut, Synthesis of nanostructured TiO_2/SiO_2 as an effective photocatalyst for degradation of acid orange, Appl. Surf. Sci. 279 (2013) 384–390.
[18] Y. Ao, J. Xu, D. Fu, X. Shen, C. Yuan, A novel magnetically separable, composite photocatalyst: Titania-coated magnetic activated carbon, Sep. Purif. Technol. 61 (2008) 436–441.
[19] J.K. Yang, S.M. Lee, M. Farrokhi, O. Giahi, M.S. Shirzad Siboni, Photocatalytic removal of Cr(VI) with illuminated TiO_2, Desalin. Water Treat. 46 (2012) 375–380.
[20] M. Shirzad Siboni, T.M. Samadi, K.J. Yang, M.S. Lee, Photocatalytic reduction of Cr(VI) and Ni(II) in aqueous solution by synthesized nanoparticle ZnO under ultraviolet light irradiation: A kinetic study, Environ. Technol. 32 (2012):1573–1579.
[21] P.F. Fu, Y. Luan, X.G. Dai, Preparation of activated carbon fibers supported TiO_2 photocatalyst and evaluation of its photocatalytic reactivity, J. Mol. Catal. A: Chem. 221 (2004) 81–88
[22] J.P. Cheng, R. Ma, M. Li, J.S. Wu, F. Liu, X.B. Zhang, Anatase nanocrystals coating on silica-coated magnetite: Role of polyacrylic acid treatment and its photocatalytic properties, Chem. Eng. J. 210 (2012) 80–86.
[23] S. Akbayrak, M. Kaya, M. Volkan, S. Özkar, Palladium(0) nanoparticles supported on silica-coated cobalt ferrite: A highly active, magnetically isolable and reusable catalyst for hydrolytic dehydrogenation of ammonia borane, Appl. Catal., B 147 (2014) 387–393.
[24] H. Zhang, R. Hou, Z. Lu, X. Duan, A novel magnetic nanocomposite involving anatase titania coating on silica-modified cobalt ferrite via lower temperature hydrolysis of a water-soluble titania precursor, Mater. Res. Bull. 44 (2009) 2000–2008.
[25] R. Benrabaa, A. Löfberg, A. Rubbens, E. Bordes-Richard, R.N. Vannier, A. Barama, Structure, reactivity and catalytic properties of nanoparticles of nickel ferrite in the dry reforming of methane, Catal. Today 203 (2013) 188–195.
[26] L. Sonali, S. Darshane, S.S. Suryavanshi, I.S. Mulla, Nanostructured nickel ferrite: A liquid petroleum gas sensor, Ceram. Int. 35 (2009) 1793–1797.
[27] M.W. Kadi, R.M. Mohamed, Synthesis and optimization of cubic $NiFe_2O_4$ nanoparticles with enhanced saturation magnetization, Ceram. Int. 40 (2014) 227–232.